Spin current between buckled atomic layers with a twist generated by locally broken inversion symmetry

Yuma Kitagawa,[1,2] Yuta Suzuki,[1,2] Shin-ichiro Tezuka,[2] and Hiroshi Akera[3]
[1]*Division of Applied Physics, Graduate School of Engineering, Hokkaido University, Sapporo, Hokkaido 060-8628, Japan*
[2]*Sensing Research & Development Department, Innovation Center, Marketing Headquarters, Yokogawa Electric Corporation, Tokyo 180-8750, Japan*
[3]*Division of Applied Physics, Faculty of Engineering, Hokkaido University, Sapporo, Hokkaido 060-8628, Japan*

(Received 5 July 2023; revised 2 September 2023; accepted 5 September 2023; published 25 September 2023)

Current-induced spin polarization (CISP), which appears when the inversion symmetry is broken, has been experimentally shown to generate spin currents. We have demonstrated in our recent theory that the antiparallel CISP in a double-quantum-well structure with the inversion symmetry can also create spin currents. In this paper we consider the sublattice-staggered CISP in a group-IV buckled atomic layer and theoretically study the spin current extracted from the spin-polarized atomic layer into another with identical structure. We derive a formula for the interlayer spin current in both the presence and the absence of the inversion symmetry and show that the interlayer spin current, in the inversion-symmetric case, additionally has a contribution from intersubband spin matrix elements due to spin degeneracy which is comparable in magnitude to that from intrasubband matrix elements. We calculate the interlayer spin current as a function of the interlayer twist angle using the tight-binding model and the Boltzmann equation in the relaxation-time approximation and choosing silicene as an example atomic layer. We show that the interlayer spin current created by the sublattice-staggered CISP in inversion-symmetric silicene is comparable in magnitude to that obtained from silicene with a 1 V/nm out-of-plane electric field applied to break the inversion symmetry. We find that the calculated interlayer spin current exhibits various features by twisting two layers. Most interesting is that the twist, which breaks the mirror symmetry to make the system chiral, gives rise to the component of the interlayer spin current with in-plane spin direction perpendicular to the CISP in addition to that parallel to the CISP.

DOI: 10.1103/PhysRevB.108.115431

I. INTRODUCTION

Interlayer twist has been shown to effectively control physical properties of atomic layer materials. The most pronounced is the appearance of superconductivity observed in a magic-angle twisted bilayer graphene [1,2]. In spintronics, the twist angle dependence of the spin-orbit coupling has been studied theoretically and experimentally in a heterostructure of graphene and transition-metal dichalcogenides [3–10]. Besides such equilibrium properties, transport properties such as charge and spin currents are expected to show interesting dependences on the twist angle. In fact a recent experiment [11] has demonstrated a strong dependence on the twist angle of the interlayer charge current. In this paper we consider the spin current, which is an important transport property in spintronics, between two atomic layers with the interlayer twist and theoretically study the dependence of the interlayer spin current on the twist angle.

One of the efficient methods to generate the spin current in nonmagnetic materials is to use the current-induced spin polarization (CISP) [12–22]. The total CISP in the whole volume appears only when the inversion symmetry is broken to create the spin splitting. In an inversion-symmetric system, on the other hand, the local CISP is present in the form of antiparallel CISP [23–27], when the inversion symmetry is locally broken, owing to the local spin polarization which a pair of degenerate states exhibits [28–35]. In our recent paper [27] we have proposed generating the spin current from this antiparallel CISP in a system with the inversion symmetry and demonstrated it in a double-quantum-well structure (DQWS). Although the local CISP in two wells of DQWS is in the opposite direction, an electrode placed on the DQWS selectively extracts the local CISP of the well in the electrode side, resulting in a nonzero spin current into the electrode. Another typical candidate for this approach is a group-IV buckled atomic layer which has an inversion-symmetric structure with sublattices A and B and therefore exhibits the sublattice-staggered CISP. This atomic layer can also produce a nonzero spin current to an attached electrode because the out-of-plane buckling in this structure places one sublattice closer to the electrode than the other.

In this study we add another atomic layer between the electrode and the atomic layer with the sublattice-staggered CISP and theoretically investigate the interlayer spin current between two identical group-IV buckled atomic layers. One layer with the current flow has the sublattice-staggered CISP which is extracted into the other layer in equilibrium with the electrode. The added atomic layer plays a role to make a better contact for an efficient extraction of CISP. In addition, the interlayer twist is expected to effectively control the interlayer spin current. In fact we show in this paper that the twist changes the magnitude and the sign of the interlayer spin current. More remarkable is that the twist gives rise to the

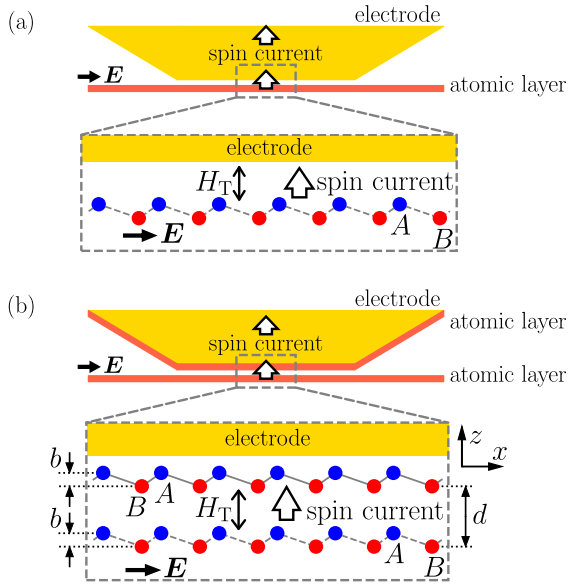

FIG. 1. (a) Side view of an atomic layer with sublattices A and B. In the presence of the in-plane electric field $\boldsymbol{E}$, the atomic layer locally exhibits the spin polarization which can be extracted into an electrode through the spin diffusion from the atomic layer. (b) Side view of the two-layer structure. The local spin polarization in the lower layer (layer l) diffuses into the upper layer (layer u) through the interlayer spin current. As shown in overall views, the spin polarization is subsequently extracted as a diffusive spin current in the electrode which can be detected, for example, by the inverse spin Hall effect.

component of the spin current with the in-plane spin direction perpendicular to the CISP. We also compare the interlayer spin current generated from this inversion-symmetric atomic layer with that from a layer with out-of-plane electric field applied to break the inversion symmetry.

This paper is organized as follows. In Sec. II we present the model and describe the Hamiltonian in the tight-binding model. In Sec. III we derive the formula for the local CISP in each of sublattices A and B using the Boltzmann equation in the relaxation-time approximation. We also derive the formula for the interlayer spin current in the second order of the interlayer tunneling perturbation. Section IV presents calculated results of the CISP and the interlayer spin current by choosing silicene as an example atomic layer. Conclusions are given in Sec. V.

II. MODEL AND HAMILTONIAN

We consider a group-IV atomic layer with the buckled honeycomb structure [36,37] [Fig. 1(a)] such as silicene [38–43], germanene [39,44], and stanene [45,46]. When the current flows in the atomic layer, staggered CISP is induced in two sublattices A and B. Owing to the buckling, the local CISP of sublattice A is extracted more than that of sublattice B by an electrode attached on the atomic layer.

To obtain a good contact between the atomic layer and the electrode in Fig. 1(a), we place another atomic layer between these two as shown in Fig. 1(b). We assume that the added layer is in equilibrium with the electrode. Then our model

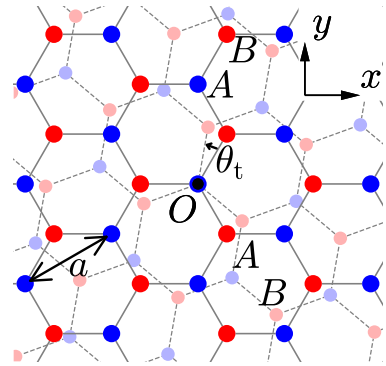

FIG. 2. Top view of the two-layer structure consisting of layer u (solid line) and layer l (dashed line).

is a two-layer structure which consists of the lower layer (layer index $\alpha = l$) with the sublattice-staggered CISP and the upper layer ($\alpha = u$) in equilibrium. The side view and the top view of the two-layer structure is shown in Figs. 1(b) and 2, respectively. These layers are the identical group-IV atomic layer with lattice constant a and buckling b. The unit cell of each layer contains two atoms $\lambda = A$ and B which constitute sublattices A and B. Layers l and u are separated by d in the z direction [Fig. 1(b)] and twisted by θ_t (Fig. 2). The two-layer structure, in the presence of twist, preserves the C_3 rotational symmetry of the group-IV atomic layer.

We employ the tight-binding model with s and p orbitals in each atom. We express the atomic basis vector of orbital X ($= s, p_x, p_y, p_z$) and spin σ ($=\uparrow, \downarrow$) by $|\boldsymbol{R}^\alpha_\lambda X\sigma\rangle$, where $\boldsymbol{R}^\alpha_\lambda$ is the position vector of an atom in sublattice λ ($= A, B$) of layer α ($= l, u$). Then the crystal basis vector of each layer is given by the sum over N atoms in the same sublattice of the same layer

$$|\alpha \boldsymbol{k} \lambda X \sigma\rangle = \frac{1}{\sqrt{N}} \sum_{\boldsymbol{R}^\alpha_\lambda} e^{i\boldsymbol{k}\cdot\boldsymbol{R}^\alpha_\lambda} |\boldsymbol{R}^\alpha_\lambda X\sigma\rangle, \tag{1}$$

where $\boldsymbol{k}$ is the two-dimensional Bloch wave vector.

We express the Hamiltonian H by

$$H = H_0 + H_T, \tag{2}$$

where H_T describes interlayer tunneling as perturbation and H_0 is the Hamiltonian of two layers without interlayer tunneling. In the unperturbed Hamiltonian H_0 we consider the nearest neighbor hopping expressed by the Slater-Koster parameter [47] and take into account the spin-orbit interaction by the LS coupling in each atom. We denote the eigenvector and eigenvalue of H_0 by $|\alpha n \boldsymbol{k}\rangle$ and $\varepsilon^\alpha_{n\boldsymbol{k}}$, respectively, where n is the band index and $|\alpha n \boldsymbol{k}\rangle$ is expressed in a linear combination of basis vectors in Eq. (1).

To demonstrate the interlayer spin current we adopt silicene and use the Slater-Koster parameter and the spin-orbit coupling strength of silicene given in Ref. [48]. Figure 3 presents the Fermi surface of two layers [Fig. 3(a)], the band structure of monolayer silicene [Fig. 3(b)], and the close-up of the conduction and valence bands in the vicinity of the K point [Fig. 3(c)]. The band structure of monolayer silicene exhibits spin degeneracy because of the presence of the inversion symmetry.

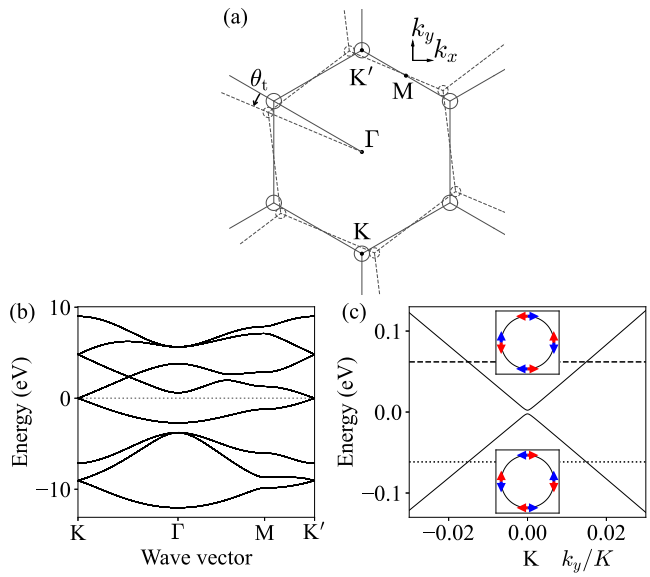

FIG. 3. Electronic states of silicene. (a) The Fermi surface of layer u (solid line) and layer l (dashed line). (b) Band structure of monolayer silicene. (c) Close-up of the conduction and valence bands in the vicinity of the K point. K [$= (2/3)(2\pi/a)$] is the distance between the K and Γ points. Insets show the in-plane component of the local spin expectation value at A (blue arrow) and B (red arrow) sublattices at an energy (indicated by dashed and dotted lines) in the conduction and valence bands.

Figure 4 presents deviations of the Fermi surface from a circle by plotting the directional dependence of the distance of the Fermi surface to the K point at four values of the Fermi energy ε_F in the conduction band. We find that the Fermi surface can be well approximated by a circle except at large values of the Fermi energy. This is also the case in the valence band.

The formula for the matrix element of H_T is given in the previous theories [49–51]. The tunneling matrix element is nonzero only when the momentum conservation $\boldsymbol{k}_u + \boldsymbol{G}_u = \boldsymbol{k}_l + \boldsymbol{G}_l$ is satisfied, where $\boldsymbol{k}_u$ and $\boldsymbol{k}_l$ ($\boldsymbol{G}_u$ and $\boldsymbol{G}_l$) are wave vectors (reciprocal lattice vectors) of layers u and l, respectively. Since the magnitude of the matrix element decays rapidly with

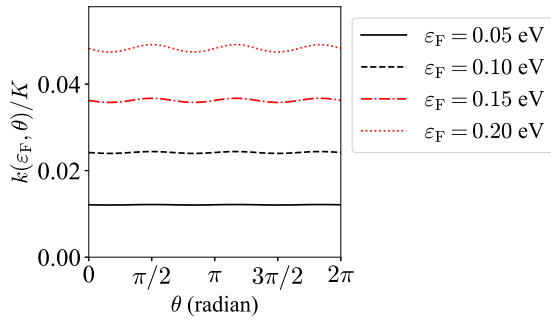

FIG. 4. Directional dependence of the distance k of the Fermi surface to the K point in monolayer silicene at four values of the Fermi energy ε_F in the conduction band. The angle θ is measured from the positive k_x direction.

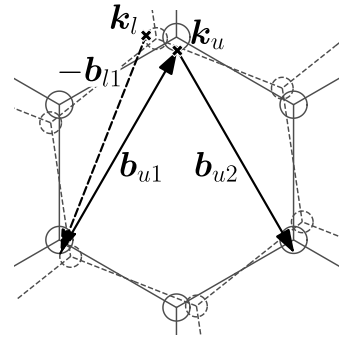

FIG. 5. Interlayer tunneling can occur between $\boldsymbol{k}_u$ and $\boldsymbol{k}_l$ (denoted by ×) near the K′ point because they satisfy the momentum conservation $\boldsymbol{k}_u = \boldsymbol{k}_l + \xi(\boldsymbol{b}_{u1} - \boldsymbol{b}_{l1})$ in Eq. (3).

increasing $|\boldsymbol{k}_u + \boldsymbol{G}_u|$, we only consider contributions from

$$\boldsymbol{k}_u = \begin{cases} \boldsymbol{k}_l, \\ \boldsymbol{k}_l + \xi(\boldsymbol{b}_{u1} - \boldsymbol{b}_{l1}), \\ \boldsymbol{k}_l - \xi(\boldsymbol{b}_{u2} - \boldsymbol{b}_{l2}), \end{cases} \tag{3}$$

where the valley index ξ is defined by $\xi = -1$ ($\xi = 1$) in the K (K′) valley and $\boldsymbol{b}_{\alpha 1}$, $\boldsymbol{b}_{\alpha 2}$ are the primitive reciprocal lattice vectors of layer α ($\boldsymbol{b}_{u1}$ and $\boldsymbol{b}_{u2}$ are shown in Fig. 5). Figure 5 shows an example of $\boldsymbol{k}_u$ and $\boldsymbol{k}_l$ near the K′ point satisfying $\boldsymbol{k}_u = \boldsymbol{k}_l + \xi(\boldsymbol{b}_{u1} - \boldsymbol{b}_{l1})$.

Except that electron densities of the two layers exactly coincide, the two-layer structure with no twist does not satisfy the momentum conservation at the Fermi energy and therefore the interlayer tunneling does not occur at absolute zero. However, in a certain range of the twist angle θ_t, the Fermi surfaces of the two layers have intersections (see, as an example, Fig. 5) where the interlayer tunneling can occur.

III. CALCULATION METHOD

A. Local current-induced spin polarization

We derive the formula for the local CISP in monolayer with electronic states described by the eigenvector $|n\boldsymbol{k}\rangle$ and the eigenvalue $\varepsilon_{n\boldsymbol{k}}$. Introducing the projection operator onto sublattice λ ($= A, B$), $P_\lambda = |\lambda\rangle\langle\lambda|$, the local spin expectation value in sublattice λ is expressed by $\langle n\boldsymbol{k}|\boldsymbol{\sigma}P_\lambda|n\boldsymbol{k}\rangle$. The global spin expectation value is $\langle n\boldsymbol{k}|\boldsymbol{\sigma}|n\boldsymbol{k}\rangle = \langle n\boldsymbol{k}|\boldsymbol{\sigma}P_A|n\boldsymbol{k}\rangle + \langle n\boldsymbol{k}|\boldsymbol{\sigma}P_B|n\boldsymbol{k}\rangle$. The local CISP is defined by

$$\langle\boldsymbol{\sigma}\rangle_\lambda = \frac{1}{S}\sum_{n\boldsymbol{k}} f_{n\boldsymbol{k}}\langle n\boldsymbol{k}|\boldsymbol{\sigma}P_\lambda|n\boldsymbol{k}\rangle \tag{4}$$

and the global CISP is given by

$$\langle\boldsymbol{\sigma}\rangle_{\text{global}} = \langle\boldsymbol{\sigma}\rangle_A + \langle\boldsymbol{\sigma}\rangle_B, \tag{5}$$

where S is the area of monolayer and $f_{n\boldsymbol{k}}$ is the distribution function. We assume $k_B T \ll \varepsilon_F$ with k_B the Boltzmann constant and take the summation over two bands at the Fermi level. To obtain $f_{n\boldsymbol{k}}$, we use the steady-state Boltzmann equation in the relaxation time approximation and in the linear response,

$$\frac{-e\boldsymbol{E}}{\hbar}\cdot\frac{\partial f_0(\varepsilon_{n\boldsymbol{k}})}{\partial\boldsymbol{k}} = -\frac{f_{n\boldsymbol{k}} - f_0(\varepsilon_{n\boldsymbol{k}})}{\tau}, \tag{6}$$

where $\boldsymbol{E}$ ($= E\boldsymbol{e}_E$ with $E = |\boldsymbol{E}|$) is the in-plane electric field, e (> 0) is the absolute value of the electron charge, $\hbar$ is the Dirac constant, $f_0(\varepsilon)$ is the Fermi distribution function, and τ is the momentum relaxation time. Because deviations of the Fermi surface from a circle are small as shown in Fig. 4, we assume the circular symmetry of the energy and the spin expectation value. Then the in-plane component of the spin expectation value is in the direction tangential to the Fermi circle and the out-of-plane component is constant on the Fermi circle.

Here we assume that τ is constant. On the other hand, if we solve the Boltzmann equation with the collision term for a particular model impurity potential, we will obtain the $\varepsilon_{\rm F}$ dependence of τ (the dependence on the spin-subband index n will be small because the spin splitting is much smaller than $\varepsilon_{\rm F}$). In this paper we do not consider the $\varepsilon_{\rm F}$ dependence because this study focuses on features of the CISP and the interlayer spin current, in which the symmetry of the system plays an important role.

First we consider an inversion-symmetric atomic layer with spin degeneracy. The summation over two degenerate states of the local spin expectation value is given, in the assumed circular symmetry, by

$$\sum_n \langle n\boldsymbol{k}|\boldsymbol{\sigma}P_\lambda|n\boldsymbol{k}\rangle = \lambda\big(\bar{\sigma}_t^{\,\beta}\boldsymbol{e}_t + \xi\bar{\sigma}_z^{\,\beta}\boldsymbol{e}_z\big). \tag{7}$$

Here λ takes 1 and -1 for sublattices A and B, respectively, while ξ takes 1 and -1 for valleys K′ and K, respectively. The unit vector $\boldsymbol{e}_t$ is in the tangential direction of the Fermi circle, defined by $\boldsymbol{e}_t = k^{-1}\boldsymbol{k}\times\boldsymbol{e}_z$, where $\boldsymbol{k}$ is the wave vector with the origin taken at the K or K′ point, $k = |\boldsymbol{k}|$, and $\boldsymbol{e}_z$ is the unit vector in the z direction. $\bar{\sigma}_t^{\,\beta}$ and $\xi\bar{\sigma}_z^{\,\beta}$, which depend on k, are the local spin expectation values in the $\boldsymbol{e}_t$ and $\boldsymbol{e}_z$ directions, respectively, of sublattice A in valley ξ of the conduction ($\beta =$ c) and valence ($\beta =$ v) bands. Both the in-plane component $\bar{\sigma}_t^{\,\beta}$, illustrated in the inset of Fig. 3(c), and the z component $\bar{\sigma}_z^{\,\beta}$ are opposite in direction between the conduction and valence bands with approximately the same magnitude: $\bar{\sigma}_t^{\rm c}(k) \approx -\bar{\sigma}_t^{\rm v}(k)$ and $\bar{\sigma}_z^{\rm c}(k) \approx -\bar{\sigma}_z^{\rm v}(k)$. The values calculated in the present tight-binding model are $\bar{\sigma}_t^{\rm c}(k) = 0.0026$ and $\bar{\sigma}_z^{\rm c}(k) = -0.021$ at $k = 0.02K$ in silicene. Substituting Eq. (7) into Eq. (4), the local CISP becomes

$$\langle\boldsymbol{\sigma}\rangle_\lambda = \frac{\lambda}{S}\sum_{\boldsymbol{k}} f_{\boldsymbol{k}}\big(\bar{\sigma}_t^{\,\beta}\boldsymbol{e}_t + \xi\bar{\sigma}_z^{\,\beta}\boldsymbol{e}_z\big), \tag{8}$$

where we have used the absence of n dependence in $f_{n\boldsymbol{k}}$ due to the spin degeneracy. Owing to the assumption of $k_{\rm B}T \ll \varepsilon_{\rm F}$, the local CISP is obtained as

$$\langle\boldsymbol{\sigma}\rangle_\lambda = \langle\sigma_\perp\rangle_\lambda\boldsymbol{e}_z\times\boldsymbol{e}_E, \tag{9}$$

with

$$\langle\sigma_\perp\rangle_\lambda = \lambda\frac{\tau\, eEk_{\rm F}\bar{\sigma}_t^{\,\beta}(k_{\rm F})}{2\pi\hbar}, \tag{10}$$

where $k_{\rm F}$ is the radius of the Fermi circle. The out-of-plane component of the local CISP is absent and the in-plane component appears in the direction perpendicular to $\boldsymbol{E}$. The local CISP in sublattices A and B are in the opposite direction and have the same magnitude. Accordingly, the global CISP is absent as expected from the inversion symmetry.

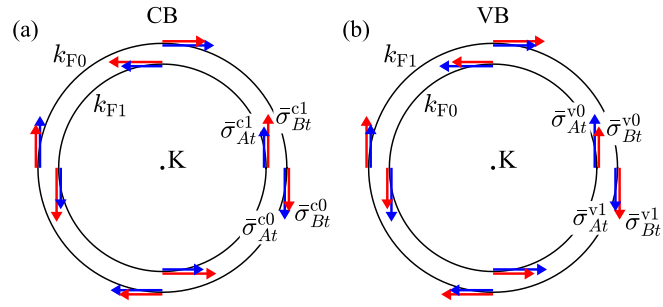

FIG. 6. Expectation value of the in-plane spin (schematic) in (a) the conduction and (b) valence bands around the K point in the globally broken inversion symmetry. The band $\nu = 0$ ($\nu = 1$) is the lower (higher) energy band.

Next we consider an atomic layer without the inversion symmetry. In the assumed circular symmetry, the local spin expectation value of band n is given by

$$\langle n\boldsymbol{k}|\boldsymbol{\sigma}P_\lambda|n\boldsymbol{k}\rangle = \bar{\sigma}_{\lambda t}^{\beta\nu}\boldsymbol{e}_t + \xi\bar{\sigma}_{\lambda z}^{\beta\nu}\boldsymbol{e}_z, \tag{11}$$

where $\bar{\sigma}_{\lambda t}^{\beta\nu}$ and $\xi\bar{\sigma}_{\lambda z}^{\beta\nu}$ are the local spin expectation values in the $\boldsymbol{e}_t$ and $\boldsymbol{e}_z$ directions, respectively, of sublattice λ in valley ξ. Here $n = (\beta,\nu)$ and the index ν is introduced to distinguish two spin-split subbands in the conduction ($\beta =$ c) and valence ($\beta =$ v) bands. The in-plane component of the local spin expectation value on the Fermi circle around the K point is schematically shown in Fig. 6. The values calculated in the present tight-binding model are $\bar{\sigma}_{At}^{\rm c0}(k) = 0.060$, $\bar{\sigma}_{Bt}^{\rm c0}(k) - \bar{\sigma}_{At}^{\rm c0}(k) = -0.0022$, $\bar{\sigma}_{Az}^{\rm c0}(k) = -0.51$, and $\bar{\sigma}_{Bz}^{\rm c0}(k) - \bar{\sigma}_{Az}^{\rm c0}(k) = 0.018$ at $k = 0.02K$ in silicene with $\Delta_{AB} = 1$ meV, where Δ_{AB} is the difference in the potential energy between sublattices, introduced to break the inversion symmetry: $-\Delta_{AB}/2$ in sublattice A and $\Delta_{AB}/2$ in sublattice B. The local CISP in the absence of the inversion symmetry is obtained as $\langle\boldsymbol{\sigma}\rangle_\lambda = \langle\sigma_\perp\rangle_\lambda\boldsymbol{e}_z\times\boldsymbol{e}_E$ with

$$\langle\sigma_\perp\rangle_\lambda = \frac{\tau\, eE}{2\pi\hbar}\sum_{\nu=0,1} k_{{\rm F}\nu}\bar{\sigma}_{\lambda t}^{\beta\nu}(k_{{\rm F}\nu}), \tag{12}$$

where $k_{{\rm F}\nu}$ is the radius of the Fermi circle in the νth subband. Because the inversion symmetry is broken, the global CISP $\langle\boldsymbol{\sigma}\rangle_{\rm global}$ arises.

B. Interlayer spin current

In this section we consider a system consisting of two layers u and l and derive the formula for the spin current between the two layers. First we define the spin angular momentum in the i direction of electrons in layer α per unit area by

$$S_\alpha^i = \frac{1}{S}{\rm tr}\left(\rho\frac{\hbar\sigma_i}{2}P_\alpha\right), \tag{13}$$

where ρ is the density operator of the two-layer system and P_α is the projection operator onto layer α defined by

$$P_\alpha = \sum_{n\boldsymbol{k}} |\alpha n\boldsymbol{k}\rangle\langle\alpha n\boldsymbol{k}|. \tag{14}$$

Then the spin angular momentum in the i direction flowing into layer α per unit area per unit time is given by

$$J^i_\alpha = \frac{dS^i_\alpha}{dt}. \tag{15}$$

As the spin direction i we take the direction parallel to $\boldsymbol{E}$ ($i = \parallel$), that perpendicular to $\boldsymbol{E}$ in the plane ($i = \perp$), and the z direction ($i = z$). In the presence of the spin-orbit coupling, the total spin angular momentum $S^i_u + S^i_l$ is not conserved (that is, $J^i_u + J^i_l \neq 0$) and therefore the spin current flowing into layer u, J^i_u, and that flowing out of layer l, $-J^i_l$, are different. However, we neglect this difference because $J^i_u + J^i_l$ is of the second order of the spin-orbit coupling. In the following we evaluate the spin current by calculating J^i_u.

We calculate J^i_u up to the second order of $H_{\rm T}$. We slowly switch on the tunneling perturbation as $H_{\rm T}e^{\eta t}$ ($\eta > 0$) and evaluate J^i_u at $t = 0$. Such adiabatic switch-on of $H_{\rm T}$ is introduced to incorporate our device geometry [Fig. 1(b)] in which layer u only partially contacts layer l and therefore wave packets describing electrons in layer l are affected by $H_{\rm T}$ within the finite contact area. The finiteness of the contact area is taken into account by a finite duration time of $H_{\rm T}$ in the wave-packet formalism. In the above switch-on model the duration time is given by η^{-1}. The finiteness of the duration time η^{-1} gives rise to an energy uncertainty $\hbar\eta$ in the interlayer transition. The interlayer spin current evaluated at $t = 0$ is written as

$$\begin{aligned} J^i_u = \frac{i}{2S}\sum_{nn''\boldsymbol{k}}\sum_{n'\boldsymbol{k}'}&\langle un\boldsymbol{k}|H_{\rm T}|ln'\boldsymbol{k}'\rangle\langle ln'\boldsymbol{k}'|H_{\rm T}|un''\boldsymbol{k}\rangle \\ &\times\left[\frac{f^l_{n'\boldsymbol{k}'} - f^u_{n\boldsymbol{k}}}{\varepsilon^l_{n'\boldsymbol{k}'} - \varepsilon^u_{n\boldsymbol{k}} + i\hbar\eta} - \frac{f^u_{n''\boldsymbol{k}} - f^l_{n'\boldsymbol{k}'}}{\varepsilon^u_{n''\boldsymbol{k}} - \varepsilon^l_{n'\boldsymbol{k}'} + i\hbar\eta}\right] \\ &\times\frac{2i\hbar\eta}{\varepsilon^u_{n''\boldsymbol{k}} - \varepsilon^u_{n\boldsymbol{k}} + 2i\hbar\eta}\langle un''\boldsymbol{k}|\sigma_i|un\boldsymbol{k}\rangle. \end{aligned} \tag{16}$$

We assume that the temperature is low enough that only the two lowest (highest) subbands $\nu = 0, 1$ in the conduction (valence) band contribute to the interlayer spin current.

Equation (16) shows that the interlayer spin current depends on the ratio of the spin splitting $|\varepsilon^u_{n''\boldsymbol{k}} - \varepsilon^u_{n\boldsymbol{k}}|$ ($n'' \neq n$) and $\hbar\eta$. When $|\varepsilon^u_{n''\boldsymbol{k}} - \varepsilon^u_{n\boldsymbol{k}}| \ll \hbar\eta$, we have

$$\frac{2i\hbar\eta}{\varepsilon^u_{n''\boldsymbol{k}} - \varepsilon^u_{n\boldsymbol{k}} + 2i\hbar\eta} \approx 1. \tag{17}$$

Then, in the limit of small η compared to the Fermi energy, we obtain

$$\begin{aligned} J^i_u = \frac{\pi}{S}\sum_{n,n',n''}\sum_{\boldsymbol{k},\boldsymbol{k}'}&\langle un\boldsymbol{k}|H_{\rm T}|ln'\boldsymbol{k}'\rangle\langle ln'\boldsymbol{k}'|H_{\rm T}|un''\boldsymbol{k}\rangle \\ &\times\delta\left(\varepsilon^l_{n'\boldsymbol{k}'} - \varepsilon^u_{n\boldsymbol{k}}\right)\left(f^l_{n'\boldsymbol{k}'} - f^u_{n\boldsymbol{k}}\right)\langle un''\boldsymbol{k}|\sigma_i|un\boldsymbol{k}\rangle. \end{aligned} \tag{18}$$

We find that intersubband matrix elements $\langle un''\boldsymbol{k}|\sigma_i|un\boldsymbol{k}\rangle$ ($n'' \neq n$) contribute to the interlayer spin current when the spin splitting is so small that $|\varepsilon^u_{n''\boldsymbol{k}} - \varepsilon^u_{n\boldsymbol{k}}| \ll \hbar\eta$.

On the other hand, when $|\varepsilon^u_{n''\boldsymbol{k}} - \varepsilon^u_{n\boldsymbol{k}}| \gg \hbar\eta$, we have

$$\frac{2i\hbar\eta}{\varepsilon^u_{n''\boldsymbol{k}} - \varepsilon^u_{n\boldsymbol{k}} + 2i\hbar\eta} \approx 0. \tag{19}$$

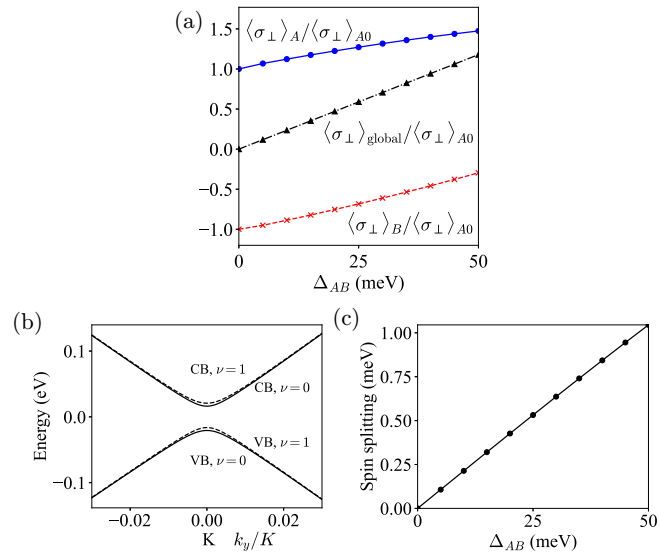

FIG. 7. (a) Local CISP $\langle\sigma_\perp\rangle_A$, $\langle\sigma_\perp\rangle_B$ and the global CISP $\langle\sigma_\perp\rangle_A + \langle\sigma_\perp\rangle_B$ as functions of Δ_{AB}, the potential difference between A and B sublattices, at $k_{\rm F0} = 0.02K$ in the conduction band. $\langle\sigma_\perp\rangle_{A0}$ is the value of $\langle\sigma_\perp\rangle_A$ at $\Delta_{AB} = 0$. (b) Spin-split energy bands at $\Delta_{AB} = 50$ meV in the vicinity of the K point. CB and VB denote the conduction band and the valence band, respectively. (c) Δ_{AB} dependence of the spin splitting at $k = 0.02K$ in the conduction band.

Then terms with $n'' \neq n$ do not contribute to the interlayer spin current and

$$J^i_u = \frac{\hbar}{2S}\sum_{n,n'}\sum_{\boldsymbol{k},\boldsymbol{k}'} W^{u,l}_{n\boldsymbol{k},n'\boldsymbol{k}'}\left(f^l_{n'\boldsymbol{k}'} - f^u_{n\boldsymbol{k}}\right)\langle un\boldsymbol{k}|\sigma_i|un\boldsymbol{k}\rangle, \tag{20}$$

where $W^{u,l}_{n\boldsymbol{k},n'\boldsymbol{k}'}$ is the transition rate given by

$$W^{u,l}_{n\boldsymbol{k},n'\boldsymbol{k}'} = \frac{2\pi}{\hbar}|\langle un\boldsymbol{k}|H_{\rm T}|ln'\boldsymbol{k}'\rangle|^2\delta\left(\varepsilon^l_{n'\boldsymbol{k}'} - \varepsilon^u_{n\boldsymbol{k}}\right). \tag{21}$$

Therefore, the interlayer spin current is expressed only by intrasubband matrix elements $\langle un\boldsymbol{k}|\sigma_i|un\boldsymbol{k}\rangle$ when the spin splitting is large enough that $|\varepsilon^u_{n''\boldsymbol{k}} - \varepsilon^u_{n\boldsymbol{k}}| \gg \hbar\eta$.

The spin current with spin in the z direction, J^z_u, is absent in a two-layer system with the C_3 rotational symmetry. This absence can be derived by noting that J^z_u does not change when the direction of the in-plane electric field is rotated by $\pm 2\pi/3$ around the z axis and that the sum of in-plane electric fields at three directions separated by $2\pi/3$ is zero.

IV. CALCULATED RESULTS

First we present the local and global CISPs of monolayer silicene calculated using the absolute-zero formula Eq. (12) for an atomic layer without the inversion symmetry. We break the inversion symmetry by introducing the potential energy $-\Delta_{AB}/2$ in sublattice A and $\Delta_{AB}/2$ in sublattice B. Calculated Δ_{AB} dependences of the local CISP $\langle\sigma_\perp\rangle_A$, $\langle\sigma_\perp\rangle_B$ and the global CISP $\langle\sigma_\perp\rangle_A + \langle\sigma_\perp\rangle_B$ are presented in Fig. 7(a). Here we place the Fermi level in the conduction band and fix the Fermi wave number of the $n = 0$ band at $k_{\rm F0} = 0.02K$, where K is the distance between the K and Γ points in Fig. 3. Because of the spin splitting present at $\Delta_{AB} > 0$ the Fermi

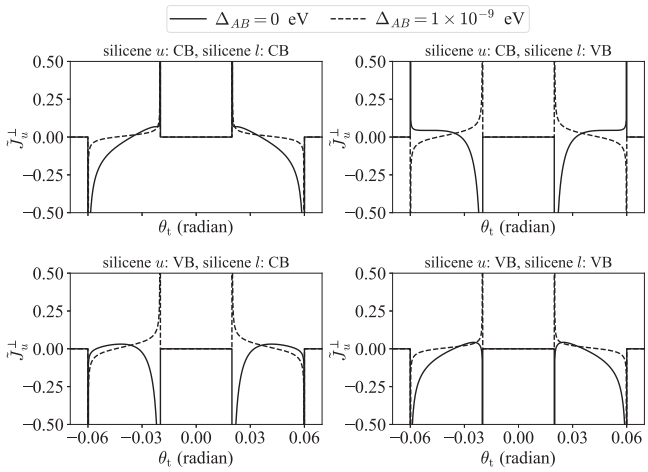

FIG. 8. Interlayer spin current $\tilde{J}_u^{\perp} = J_u^{\perp}/J_0$ as a function of the twist angle θ_t. $J_0 = \tau\, eEk_0 V^0_{pp\pi}/(4\pi\hbar)$, where $V^0_{pp\pi}$ is $|V_{pp\pi}|$ between the nearest neighbor atoms in monolayer silicene and $k_0 = 0.02K$. The Fermi wave numbers k_{Fu} and k_{Fl} of layers u and l are chosen to be $k_{Fu} = 0.04K$ and $k_{Fl} = 0.02K$, respectively.

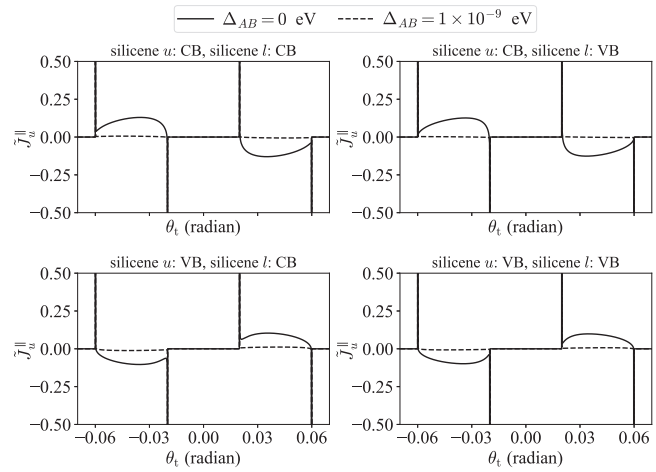

FIG. 9. Interlayer spin current $\tilde{J}_u^{\parallel} = J_u^{\parallel}/J_0$ as a function of the twist angle θ_t. See Fig. 8 for more explanation.

wave number of the $n = 1$ band, k_{F1}, is smaller than k_{F0} in the conduction band [Fig. 7(b)] and the electron density decreases with increasing Δ_{AB}. However, the change of the electron density within $0 < \Delta_{AB} \leqslant 50$ meV is negligible since the spin splitting is small compared to the Fermi energy at $\Delta_{AB} \leqslant 50$ meV [Fig. 7(c)]. The electron density at $k_F = 0.02K$ is 1.5×10^{12} cm^{-2}, which can be reached in a typical graphene experiment [52].

As shown in Fig. 7(a), the magnitude of the local CISP is comparable to that of the global CISP in the region of $\Delta_{AB} < 50$ meV. The global CISP, $\langle\sigma_\perp\rangle_A + \langle\sigma_\perp\rangle_B$, which increases with Δ_{AB}, reaches the value of the local CISP, $\langle\sigma_\perp\rangle_A$ (at $\Delta_{AB} = 0$), around $\Delta_{AB} = 50$ meV, which corresponds to the potential difference generated by the out-of-plane electric field of the order of 1 V/nm, nearly the maximum value realized in experiment [53]. This suggests that the spin current created by the local CISP in a system with inversion symmetry ($\Delta_{AB} = 0$) can be comparable to that obtained from the global CISP in a system with strongly broken inversion symmetry.

Now we present, in Figs. 8 and 9, the interlayer spin current between two silicene layers calculated at $T = 0$ using Eqs. (18) and (20). In calculating the interlayer spin current we have assumed the circular Fermi surface as in the calculation of the CISP in Sec. III A and additionally used the linear-in-k dependence of the energy in evaluating $\delta(\varepsilon^l_{n'\boldsymbol{k}'} - \varepsilon^u_{n\boldsymbol{k}})$. In contrast to the CISP calculation, we have used numerical eigenvectors to obtain matrix elements of σ_i as well as those of H_T. In calculating matrix elements of H_T we have used the interlayer distance $d = 3.19$ Å of bilayer silicene [54] and the decay length of the interlayer hopping amplitude $0.184a$ used in the calculation of bilayer graphene [51,55].

The interlayer spin current with the spin direction perpendicular to the in-plane electric field $\boldsymbol{E}$, $J_u^{\perp}$, is presented in Fig. 8, while that with the spin direction parallel to $\boldsymbol{E}$, $J_u^{\parallel}$, is presented in Fig. 9. Each figure shows spin currents calculated in four different cases where the Fermi level in each of u and l layers is placed in either the conduction or valence band. In all cases the Fermi wave number is chosen to be $k_{Fu} = 0.04K$ in layer u and $k_{Fl} = 0.02K$ in layer l. In each case the interlayer spin current is plotted as a function of θ_t, the twist angle defined in Fig. 2. Solid and dashed lines show the interlayer spin current in the presence of the spin degeneracy ($\Delta_{AB} = 0$) [Eq. (18)] and that in its absence [Eq. (20)], respectively. To remove the spin degeneracy without appreciably changing electronic states, we have chosen the value of $\Delta_{AB} = 1\times10^{-9}$ eV in the latter case.

When two layers are twisted ($\theta_t \neq 0$), the parallel-to-$\boldsymbol{E}$ spin component, $J_u^{\parallel}$, appears as demonstrated in Fig. 9. This is in contrast to the monolayer CISP which is induced only in the direction $\boldsymbol{e}_z \times \boldsymbol{e}_E$ that is perpendicular to $\boldsymbol{E}$. The appearance of $J_u^{\parallel}$ is caused by the disappearance at $\theta_t \neq 0$ of the mirror symmetry with respect to the plane including $\boldsymbol{E}$ and $\boldsymbol{e}_z$. In other words, the *chirality* of the twisted-two-layer structure gives rise to the spin current between two layers with the spin *perpendicular to the CISP* in layer l. The interlayer spin current is present only in the region of θ_t where the Fermi circles of two layers have intersecting points so that the momentum conservation Eq. (3) can be satisfied at the Fermi level. At the boundary of the θ_t region the interlayer spin current diverges because the number of interlayer transitions satisfying the momentum conservation diverges when the two Fermi circles touch. We also find that $J_u^{\perp}(\theta_t)$ and $J_u^{\parallel}(\theta_t)$ are even and odd functions of θ_t.

We notice, in these plots as a function of θ_t, that the interlayer spin current reverses the sign with changing θ_t. The interlayer spin current is the sum of contributions from different intersections of Fermi circles of two layers (Fig. 5), $\boldsymbol{k}$ and $\boldsymbol{k}'$, which move on each Fermi circle as θ_t changes. The sign of each contribution in the case of no spin degeneracy [Eq. (20)] is determined by the sign of the spin expectation value $\langle u n\boldsymbol{k}|\sigma_i|u n\boldsymbol{k}\rangle$ ($i = \perp, \parallel$) and that of the distribution function $f^l_{n'\boldsymbol{k}'} - f^u_{n\boldsymbol{k}} (\propto \boldsymbol{E}\cdot\boldsymbol{k}')$. These signs depend on directions of $\boldsymbol{k}$ and $\boldsymbol{k}'$ from the center of each Fermi circle. Such dependences on directions of $\boldsymbol{k}$ and $\boldsymbol{k}'$ give the sign reversal of the interlayer spin current with changing θ_t.

Interestingly, we find in both Figs. 8 and 9 that the interlayer spin current in the presence of spin degeneracy (solid line) and that in its absence (dashed line) are significantly different despite a negligible difference in the value of Δ_{AB}. This shows that intersubband spin matrix elements, which appear only in the formula Eq. (18) for the presence of spin degeneracy, play an important role. Such a considerable contribution from intersubband matrix elements of in-plane spin, $\sigma_\perp$ and $\sigma_\parallel$, can be understood by noting that the spin, in the spin-split subbands $n = 0$ and 1, orients approximately the positive z and negative z directions as we have presented in Sec. III A.

Which of the spin-degenerate formula Eq. (18) and the spin-nondegenerate formula Eq. (20) applies is determined by whether the magnitude of the spin splitting is smaller or larger than $\hbar\eta$. Here we estimate η in a two-layer system employed in the previous experiment [11]. In this system layer u contacts layer l in a region of 1 μm. The inverse of η, which is the duration time of the tunneling perturbation $H_{\rm T}$, corresponds in this system to the time span for an electron in layer l to pass under the contact region. Using the group velocity at $k_{\rm F} = 0.02K$, 6×10^5 m/s, η^{-1} is estimated to be 2×10^{-12} s, which gives $\hbar\eta \approx 0.4$ meV. Then the spin-degenerate formula Eq. (18) applies for the spin splitting much smaller than 0.4 meV, which corresponds to $\Delta_{AB} \ll 20$ meV [see Fig. 7(c)].

Finally we show that the interlayer spin current extracted from the local CISP in the inversion symmetric silicene is comparable to that from the CISP in silicene with a large electric field applied perpendicular to the layer. We have examined the Δ_{AB} dependence of $J_u^\perp$ and $J_u^\parallel$ in four choices of the Fermi level location, the conduction or valence band in each layer. Then we find that the typical value of $|J_u^\perp|$ and $|J_u^\parallel|$ at $\Delta_{AB} = 100$ meV, corresponding to the electric field of 1 V/nm, is of the same order of that produced by the inversion symmetric silicene at $\Delta_{AB} = 0$.

V. CONCLUSIONS

We have considered a two-layer system consisting of identical group-IV buckled atomic layers and theoretically studied the interlayer spin current generated by the monolayer CISP in one of the two layers as a function of the interlayer twist angle. Although the total CISP is zero in this atomic layer with inversion symmetry, sublattices A and B locally exhibit the staggered CISP, from which a nonzero interlayer spin current is obtained owing to the out-of-plane buckling with sublattice A closer to the other layer than sublattice B.

We have derived the formula for the interlayer spin current in the second order of the interlayer tunneling perturbation. The derived formula depends on whether the spin degeneracy is present or not—more precisely whether the spin splitting is smaller or larger than the energy uncertainty brought by the finite duration time of the tunneling perturbation. The spin-degenerate formula includes both the intersubband and intrasubband matrix elements of the spin operator, while the spin-nondegenerate formula only has the intrasubband matrix element. We have found that the contribution from this intersubband spin matrix element in the spin-degenerate case makes the calculated interlayer spin current markedly different from that in the spin-nondegenerate case.

We have calculated the interlayer spin current using the tight-binding model and the Boltzmann equation in the relaxation-time approximation by choosing silicene as an example atomic layer. We have found that the interlayer spin current created by the sublattice-staggered CISP in inversion-symmetric silicene is comparable in magnitude to that obtained from silicene with a 1 V/nm out-of-plane electric field applied to break the inversion symmetry. This result is consistent with the calculated CISP in sublattices A and B, which shows that the CISP of each sublattice in inversion-symmetric silicene is comparable in magnitude to that in silicene with inversion symmetry broken.

The calculated interlayer spin current exhibits various features by twisting two layers: it is switched on and off, diverges to infinity, and reverses its sign as the twist angle changes. Most interestingly the twist, which breaks the mirror symmetry to make the system chiral, gives rise to the component of the interlayer spin current with in-plane spin direction perpendicular to the CISP in addition to that parallel to the CISP.

ACKNOWLEDGMENT

This work was partly supported by a Grant-in-Aid for Scientific Research (C) Grant No. JP21K03413 from the Japan Society for the Promotion of Science (JSPS).

[1] Y. Cao, V. Fatemi, S. Fang, K. Watanabe, T. Taniguchi, E. Kaxiras, and P. Jarillo-Herrero, Unconventional superconductivity in magic-angle graphene superlattices, Nature (London) **556**, 43 (2018).

[2] M. Yankowitz, S. Chen, H. Polshyn, Y. Zhang, K. Watanabe, T. Taniguchi, D. Graf, A. F. Young, and C. R. Dean, Tuning superconductivity in twisted bilayer graphene, Science **363**, 1059 (2019).

[3] A. M. Alsharari, M. M. Asmar, and S. E. Ulloa, Topological phases and twisting of graphene on a dichalcogenide monolayer, Phys. Rev. B **98**, 195129 (2018).

[4] Y. Li and M. Koshino, Twist-angle dependence of the proximity spin-orbit coupling in graphene on transition-metal dichalcogenides, Phys. Rev. B **99**, 075438 (2019).

[5] A. David, P. Rakyta, A. Kormányos, and G. Burkard, Induced spin-orbit coupling in twisted graphene–transition metal dichalcogenide heterobilayers: Twistronics meets spintronics, Phys. Rev. B **100**, 085412 (2019).

[6] T. Naimer, K. Zollner, M. Gmitra, and J. Fabian, Twist-angle dependent proximity induced spin-orbit coupling in graphene/transition metal dichalcogenide heterostructures, Phys. Rev. B **104**, 195156 (2021).

[7] A. Pezo, Z. Zanolli, N. Wittemeier, P. Ordejón, A. Fazzio, S. Roche, and J. H. Garcia, Manipulation of spin transport in graphene/transition metal dichalcogenide heterobilayers upon twisting, 2D Mater. **9**, 015008 (2022).

[8] C. G. Péterfalvi, A. David, P. Rakyta, G. Burkard, and A. Kormányos, Quantum interference tuning of spin-orbit

coupling in twisted van der Waals trilayers, Phys. Rev. Res. **4**, L022049 (2022).

[9] A. Veneri, D. T. S. Perkins, C. G. Péterfalvi, and A. Ferreira, Twist angle controlled collinear Edelstein effect in van der Waals heterostructures, Phys. Rev. B **106**, L081406 (2022).

[10] S. Lee, D. J. P. de Sousa, Y.-K. Kwon, F. de Juan, Z. Chi, F. Casanova, and T. Low, Charge-to-spin conversion in twisted graphene/WSe_2 heterostructures, Phys. Rev. B **106**, 165420 (2022).

[11] A. Inbar, J. Birkbeck, J. Xiao, T. Taniguchi, K. Watanabe, B. Yan, Y. Oreg, A. Stern, E. Berg, and S. Ilani, The quantum twisting microscope, Nature (London) **614**, 682 (2023).

[12] V. Edelstein, Spin polarization of conduction electrons induced by electric current in two-dimensional asymmetric electron systems, Solid State Commun. **73**, 233 (1990).

[13] Y. K. Kato, R. C. Myers, A. C. Gossard, and D. D. Awschalom, Coherent spin manipulation without magnetic fields in strained semiconductors, Nature (London) **427**, 50 (2004).

[14] Y. K. Kato, R. C. Myers, A. C. Gossard, and D. D. Awschalom, Current-Induced Spin Polarization in Strained Semiconductors, Phys. Rev. Lett. **93**, 176601 (2004).

[15] A. Y. Silov, P. A. Blajnov, J. H. Wolter, R. Hey, K. H. Ploog, and N. S. Averkiev, Current-induced spin polarization at a single heterojunction, Appl. Phys. Lett. **85**, 5929 (2004).

[16] N. P. Stern, S. Ghosh, G. Xiang, M. Zhu, N. Samarth, and D. D. Awschalom, Current-Induced Polarization and the Spin Hall Effect at Room Temperature, Phys. Rev. Lett. **97**, 126603 (2006).

[17] C. L. Yang, H. T. He, L. Ding, L. J. Cui, Y. P. Zeng, J. N. Wang, and W. K. Ge, Spectral Dependence of Spin Photocurrent and Current-Induced Spin Polarization in an InGaAs/InAlAs Two-Dimensional Electron Gas, Phys. Rev. Lett. **96**, 186605 (2006).

[18] A. Dyrdał, J. Barnaś, and V. K. Dugaev, Current-induced spin polarization in graphene due to Rashba spin-orbit interaction, Phys. Rev. B **89**, 075422 (2014).

[19] M. Offidani, M. Milletarì, R. Raimondi, and A. Ferreira, Optimal Charge-to-Spin Conversion in Graphene on Transition-Metal Dichalcogenides, Phys. Rev. Lett. **119**, 196801 (2017).

[20] K. Kondou, H. Tsai, H. Isshiki, and Y. Otani, Efficient spin current generation and suppression of magnetic damping due to fast spin ejection from nonmagnetic metal/indium-tin-oxide interfaces, APL Mater. **6**, 101105 (2018).

[21] T. S. Ghiasi, A. A. Kaverzin, P. J. Blah, and B. J. Van Wees, Charge-to-spin conversion by the Rashba–Edelstein effect in two-dimensional van der Waals heterostructures up to room temperature, Nano Lett. **19**, 5959 (2019).

[22] L. A. Benítez, W. Savero Torres, J. F. Sierra, M. Timmermans, J. H. Garcia, S. Roche, M. V. Costache, and S. O. Valenzuela, Tunable room-temperature spin galvanic and spin Hall effects in van der Waals heterostructures, Nat. Mater. **19**, 170 (2020).

[23] Y. Yanase, Magneto-electric effect in three-dimensional coupled zigzag chains, J. Phys. Soc. Jpn. **83**, 014703 (2014).

[24] J. Železný, H. Gao, K. Výborný, J. Zemen, J. Mašek, A. Manchon, J. Wunderlich, J. Sinova, and T. Jungwirth, Relativistic Néel-Order Fields Induced by Electrical Current in Antiferromagnets, Phys. Rev. Lett. **113**, 157201 (2014).

[25] P. Wadley, B. Howells, J. Železný, C. Andrews, V. Hills, R. P. Campion, V. Novák, K. Olejník, F. Maccherozzi, S. S. Dhesi, S. Y. Martin, T. Wagner, J. Wunderlich, F. Freimuth, Y. Mokrousov, J. Kuneš, J. S. Chauhan, M. J. Grzybowski, A. W. Rushforth, K. W. Edmonds, B. L. Gallagher *et al.*, Electrical switching of an antiferromagnet, Science **351**, 587 (2016).

[26] H. Watanabe and Y. Yanase, Symmetry analysis of current-induced switching of antiferromagnets, Phys. Rev. B **98**, 220412(R) (2018).

[27] Y. Suzuki, Y. Kitagawa, S.-i. Tezuka, and H. Akera, Spin-current generation from local spin polarization induced by current through local inversion asymmetry: Double quantum well structure, Phys. Rev. B **107**, 115306 (2023).

[28] X. Zhang, Q. Liu, J.-W. Luo, A. J. Freeman, and A. Zunger, Hidden spin polarization in inversion-symmetric bulk crystals, Nat. Phys. **10**, 387 (2014).

[29] J. M. Riley, F. Mazzola, M. Dendzik, M. Michiardi, T. Takayama, L. Bawden, C. Granerød, M. Leandersson, T. Balasubramanian, M. Hoesch, T. K. Kim, H. Takagi, W. Meevasana, P. Hofmann, M. Bahramy, J. Wells, and P. C. King, Direct observation of spin-polarized bulk bands in an inversion-symmetric semiconductor, Nat. Phys. **10**, 835 (2014).

[30] M. Gehlmann, I. Aguilera, G. Bihlmayer, E. Młyńczak, M. Eschbach, S. Döring, P. Gospodarič, S. Cramm, B. Kardynał, L. Plucinski, S. Blügel, and C. M. Schneider, Quasi 2D electronic states with high spin-polarization in centrosymmetric MoS_2 bulk crystals, Sci. Rep. **6**, 26197 (2016).

[31] W. Yao, E. Wang, H. Huang, K. Deng, M. Yan, K. Zhang, K. Miyamoto, T. Okuda, L. Li, Y. Wang, H. Gao, C. Liu, W. Duan, and S. Zhou, Direct observation of spin-layer locking by local Rashba effect in monolayer semiconducting $PtSe_2$ film, Nat. Commun. **8**, 14216 (2017).

[32] E. Razzoli, T. Jaouen, M.-L. Mottas, B. Hildebrand, G. Monney, A. Pisoni, S. Muff, M. Fanciulli, N. C. Plumb, V. A. Rogalev, V. N. Strocov, J. Mesot, M. Shi, J. H. Dil, H. Beck, and P. Aebi, Selective Probing of Hidden Spin-Polarized States in Inversion-Symmetric Bulk MoS_2, Phys. Rev. Lett. **118**, 086402 (2017).

[33] S.-L. Wu, K. Sumida, K. Miyamoto, K. Taguchi, T. Yoshikawa, A. Kimura, Y. Ueda, M. Arita, M. Nagao, S. Watauchi, I. Tanaka, and T. Okuda, Direct evidence of hidden local spin polarization in a centrosymmetric superconductor $LaO_{0.55}F_{0.45}BiS_2$, Nat. Commun. **8**, 1919 (2017).

[34] C. Cheng, J.-T. Sun, X.-R. Chen, and S. Meng, Hidden spin polarization in the 1t-phase layered transition-metal dichalcogenides MX_2 (M=Zr, Hf; X=S, Se, Te), Sci. Bull. **63**, 85 (2018).

[35] L. Yuan, Q. Liu, X. Zhang, J.-W. Luo, S.-S. Li, and A. Zunger, Uncovering and tailoring hidden Rashba spin-orbit splitting in centrosymmetric crystals, Nat. Commun. **10**, 906 (2019).

[36] S. Balendhran, S. Walia, H. Nili, S. Sriram, and M. Bhaskaran, Elemental analogues of graphene: Silicene, germanene, stanene, and phosphorene, Small **11**, 640 (2015).

[37] A. Molle, J. Goldberger, M. Houssa, Y. Xu, S.-C. Zhang, and D. Akinwande, Buckled two-dimensional Xene sheets, Nat. Mater. **16**, 163 (2017).

[38] S. Cahangirov, M. Topsakal, E. Aktürk, H. Şahin, and S. Ciraci, Two- and One-Dimensional Honeycomb Structures of Silicon and Germanium, Phys. Rev. Lett. **102**, 236804 (2009).

[39] E. Scalise, M. Houssa, G. Pourtois, B. van den Broek, V. Afanas'ev, and A. Stesmans, Vibrational properties of silicene and germanene, Nano Res. **6**, 19 (2013).

[40] G. G. Guzmán-Verri and L. C. Lew Yan Voon, Electronic structure of silicon-based nanostructures, Phys. Rev. B **76**, 075131 (2007).

[41] P. Vogt, P. De Padova, C. Quaresima, J. Avila, E. Frantzeskakis, M. C. Asensio, A. Resta, B. Ealet, and G. Le Lay, Silicene: Compelling Experimental Evidence for Graphene-like Two-Dimensional Silicon, Phys. Rev. Lett. **108**, 155501 (2012).

[42] M. Houssa, A. Dimoulas, and A. Molle, Silicene: A review of recent experimental and theoretical investigations, J. Phys.: Condens. Matter **27**, 253002 (2015).

[43] B. Feng, Z. Ding, S. Meng, Y. Yao, X. He, P. Cheng, L. Chen, and K. Wu, Evidence of silicene in honeycomb structures of silicon on Ag(111), Nano Lett. **12**, 3507 (2012).

[44] M. E. Dávila, L. Xian, S. Cahangirov, A. Rubio, and G. Le Lay, Germanene: A novel two-dimensional germanium allotrope akin to graphene and silicene, New J. Phys. **16**, 095002 (2014).

[45] Y. Xu, B. Yan, H.-J. Zhang, J. Wang, G. Xu, P. Tang, W. Duan, and S.-C. Zhang, Large-Gap Quantum Spin Hall Insulators in Tin Films, Phys. Rev. Lett. **111**, 136804 (2013).

[46] F.-F. Zhu, W.-J. Chen, Y. Xu, C.-L. Gao, D.-D. Guan, C.-H. Liu, D. Qian, S.-C. Zhang, and J.-F. Jia, Epitaxial growth of two-dimensional stanene, Nat. Mater. **14**, 1020 (2015).

[47] J. C. Slater and G. F. Koster, Simplified LCAO method for the periodic potential problem, Phys. Rev. **94**, 1498 (1954).

[48] C.-C. Liu, H. Jiang, and Y. Yao, Low-energy effective Hamiltonian involving spin-orbit coupling in silicene and two-dimensional germanium and tin, Phys. Rev. B **84**, 195430 (2011).

[49] R. Bistritzer and A. H. MacDonald, Transport between twisted graphene layers, Phys. Rev. B **81**, 245412 (2010).

[50] R. Bistritzer and A. H. MacDonald, Moire bands in twisted double-layer graphene, Proc. Natl. Acad. Sci. USA **108**, 12233 (2011).

[51] M. Koshino, Interlayer interaction in general incommensurate atomic layers, New J. Phys. **17**, 015014 (2015).

[52] S. Das Sarma, S. Adam, E. H. Hwang, and E. Rossi, Electronic transport in two-dimensional graphene, Rev. Mod. Phys. **83**, 407 (2011).

[53] Y. Zhang, T.-T. Tang, C. Girit, Z. Hao, M. C. Martin, A. Zettl, M. F. Crommie, Y. R. Shen, and F. Wang, Direct observation of a widely tunable bandgap in bilayer graphene, Nature (London) **459**, 820 (2009).

[54] F. Liu, C.-C. Liu, K. Wu, F. Yang, and Y. Yao, $d + id'$ Chiral Superconductivity in Bilayer Silicene, Phys. Rev. Lett. **111**, 066804 (2013).

[55] G. Trambly de Laissardière, D. Mayou, and L. Magaud, Localization of Dirac electrons in rotated graphene bilayers, Nano Lett. **10**, 804 (2010).